Numerical simulation of flow around circular cylinder near a plane wall: effects of wall proximity, boundary layer and reynolds number

DOI: 10.46932/sfjdv4n5-021

Received on: July 27th, 2023
Accepted on: August 25th, 2023

Mauro Grioni
Doctor in Engineering Sciences
Institution: National University of Cuyo and National Scientific and Technical Research Council (CONICET)
Address: University Center, Mendoza, 5500, Argentina
E-mail: mauro.grioni@ingenieria.uncuyo.edu.ar

Sergio Elaskar
Doctor in Aerospace Engineering and Engineering Sciences
Institution: National University of Córdoba and National Scientific and Technical Research Council (CONICET)
Address: Av. Velez Sarfield 1611, Córdoba, Argentina
E-mail: selaskar@unc.edu.ar

Anibal Edmundo Mirasso
Doctor in Engineering Sciences
Institution: National University of Cuyo
Address: University Center, Mendoza, 5500, Argentina
E-mail: anibal.mirasso@ingenieria.uncuyo.edu.ar

ABSTRACT
The cylindrical structures in close proximity to a solid surface have diverse and numerous applications within current engineering. While the flow dynamics around an isolated circular cylinder located in a uniform flow are reasonably well understood, this is not the case when the cylinder is positioned near a plane wall. This particular configuration is studied using computational fluid dynamics (CFD) through the Fluent code, which implements the finite volume method. For this purpose, a two-dimensional and transient flow is carry out using the SST-SAS turbulence model. The effects of changing the separation (G) between the cylinder (with diameter D) and the wall are analyzed for different Reynolds numbers and different boundary layer thicknesses. The lift and drag coefficients and the behavior of vortex shedding (Strouhal number, St) are examined. The numerical results are compared with values available in the literature from experimental wind tunnel tests, showing that both the drag and lift coefficients strongly depend on the separation ratio (G/D) and are affected by the boundary layer thicknesses.

Keywords*:* circular cylinder, vortex shedding, SST-SAS turbulence model.

1 INTRODUCTION

Flow around a cylinder has been extensively studied due to its simple geometry and wide-ranging engineering applications. However, when a cylinder is positioned near a plane wall, the proximity introduces additional complexity to the flow patterns compared to an isolated cylinder. This flow primarily

depends on three parameters: Reynolds number (Re), boundary layer thickness (δ), and gap height (G) between the bottom of the cylinder and the wall. This study aims to investigate the influence of these three parameters on the flow around a cylinder near the ground.

Over the past decades, numerous experimental studies have been conducted on circular cylinders near the floor at moderately high Reynolds numbers (Re = 103-105, based on free-stream velocity U and cylinder diameter D). Bearman and Zdravkovich (1978) observed that the forces on the cylinder strongly depend on the separation (G) when approaching the wall, and vortex shedding suppression occurs when the separation falls below a critical distance. Taniguchi and Miyakoshi (1990) conducted further experiments and confirmed the significant impact of wall proximity on the flow patterns and forces. Buresti and Lanciotti (1992) investigated the effects of different boundary layer thicknesses on the flow characteristics around cylinders near the ground, highlighting the complex interaction between the boundary layer and the cylinder. Lei et al. (1999) also explored the phenomenon of vortex shedding suppression and its correlation with the separation ratio.

In the field of computational fluid dynamics (CFD), efforts have been made to accurately simulate the flow around cylinders near walls. Traditional approaches, such as Reynolds-averaged Navier-Stokes (RANS) simulations, have limitations in capturing the large-scale wake structures accurately. Spalart (2000) discussed the challenges of direct numerical simulations (DNS) due to their computational requirements, especially for complex flow configurations. To address these challenges, Strelets (2001) proposed the Detached Eddy Simulation (DES) methodology, which combines aspects of RANS and large eddy simulation (LES) to achieve improved accuracy for complex flow phenomena near walls. Menter et al. (2003) introduced the Scale-Adaptive Simulation (SAS) model as an alternative, which offers a computationally efficient approach to capture unsteady features of the flow while providing accurate results for regions influenced by the boundary layer. The SAS approach was used previously to solve the wake around one cylinder, and the interaction between two cylinders with satisfactory results by Grioni et al. (2017, 2018a,b, 2019, 2020).

The main objective of this study is to examine the accuracy of the SST-SAS turbulence model in reproducing the cessation of von-Karman vortex shedding and its impact on the lift and drag coefficients of the cylinder near a plane wall for a two-dimensional model. The obtained results will be compared with experimental data from Buresti and Lanciotti (1992) to validate the model's performance and contribute to our understanding of the intricate flow behavior near the cylinder-wall configuration.

The paper is organized into five sections. The second section briefly describes governing equation and the equations derived from the SST-SAS turbulence model. Section 3 describes the numerical methodology to evaluate the flow around circular cylinder near a plane wall. In Section 4, results of numerical simulation are presented. Finally, in Section 5 there are the main conclusions.

2 GOVERNING EQUATIONS

For this work, the governing equations for the analyzed flows are the continuity and the Navier-Stokes equations for a constant-density, isothermal and incompressible flow, which after ensemble averaging obtain the following unsteady Reynolds averaged Navier-Stokes (URANS) system expressed in the Cartesian system of coordinates (*O, x1, x2, x3*):

$$\frac{\partial \langle u_i \rangle}{\partial x_i} = 0 \qquad (1)$$

$$\frac{\partial \langle u_i \rangle}{\partial t} + \frac{\partial \langle u_i \rangle \langle u_j \rangle}{\partial x_j} = -\frac{1}{\rho}\frac{\partial \langle p \rangle}{\partial x_i} + \frac{\partial}{\partial x_j}\left[\upsilon\left(\frac{\partial \langle u_i \rangle}{\partial x_j} + \frac{\partial \langle u_j \rangle}{\partial x_i}\right) - \langle u_i' u_j' \rangle\right] \qquad (2)$$

Where,

$\langle u_i \rangle$ is the ensemble average component of the velocity in the direction x_i, ρ is the density of the fluid, p is the ensemble average pressure, υ is the dynamic viscosity.

As a result of Reynolds averaging, additional terms ($\langle u_i' u_j' \rangle$) are introduced into the Navier-Stokes equations. These terms, known as Reynolds stresses, need to be modeled. To close the above set of equations (Eqs. (1) and (2)), the Reynolds stress tensor is expressed through a Boussinesq hypothesis, namely

$$\langle u_i' u_j' \rangle = -\upsilon_t\left(\frac{\partial \langle u_i \rangle}{\partial x_j} + \frac{\partial \langle u_j \rangle}{\partial x_i}\right) + \frac{2}{3}k\delta_{ij} \qquad (3)$$

Where,

υ_t is the turbulent eddy viscosity and *k* the turbulence kinetic energy that are calculated by means of the SST-SAS turbulence model.

The SST (Shear Stress Transport) model was formulated by Menter (1994) to combine the best characteristics of the *k*-*ω* and *k*-ε model, and also to lead to significant improvements in the prediction of adverse pressure gradient flows. When the SST model is used in transient simulations, a common issue arises where this model produces overly large turbulent structures and consequently high turbulence

viscosities (Menter and Egorov, 2005; Grioni et al 2022a). To solve this, Menter and coauthors developed the SAS approach (Menter et al., 2003) and adapted it to the SST model. The resulting SST-SAS model (Menter and Egorov, 2005; Egorov and Menter, 2008; Menter and Egorov, 2010) distinguishes itself from the original SST model by the addition of a SAS term into the equation of the turbulence frequency ω, leaving unchanged the equation for the turbulence kinetic energy k. The additional source term (Q_{SAS}) is given as:

$$Q_{SAS} = \max\left[\rho\eta_2\kappa S^2\left(\frac{L}{L_{vK}}\right)^2 - C_{SAS}\frac{2\rho k}{\sigma_\Phi}\max\left(\frac{1}{\omega}\frac{\partial\omega}{\partial x_j}\frac{\partial\omega}{\partial x_j}, \frac{1}{k}\frac{\partial k}{\partial x_j}\frac{\partial k}{\partial x_j}\right), 0\right] \quad (4)$$

Where,

The model parameters are given by $\eta_2 = 3.51$, $\sigma_\Phi = 2/3$, and $C_{SAS} = 2$. The turbulence length scale (L) is calculated as:

$$L = \frac{\sqrt{k}}{c_\mu^{0.25}\omega} \quad (5)$$

The von Karman length-scale L_{vK} acts as a sensor to detect the flow unsteadiness susceptibility in the resolved velocity field, which is defined as:

$$L_{vK} = \kappa\sqrt{\left|\frac{\left(\frac{\partial\langle u_i\rangle}{\partial x_j}\right)\left(\frac{\partial\langle u_j\rangle}{\partial x_i}\right)}{\left(\frac{\partial^2\langle u_i\rangle}{\partial x^2{}_j}\right)\left(\frac{\partial^2\langle u_j\rangle}{\partial x^2{}_i}\right)}\right|} \quad (6)$$

Where,

κ is the von Karman constant.

3 NUMERICAL SIMULATION

The simulations are performed using the CFD code Ansys Fluent 2021, which implements the finite volume method to solve the equations of incompressible turbulent flow. The equations are spatially discretized using a second-order scheme for pressure and turbulence, a bounded central difference scheme

for momentum, while the temporal discretization of the equations is based on a bounded second-order implicit scheme. The resulting system of equations is iteratively solved using the segregated solver, where the SIMPLE algorithm (*Semi Implicit Method for Pressure Linked Equations*) (Patankar, 1980) is used to derive the pressure correction equations. Results obtained in Grioni et al. (2022b) proved the SIMPLE exhibits acceptable performance in resolving unsteady turbulent flow around a circular cylinder and requires less computational time compared to the SIMPLEC and PISO approaches when using the SST-SAS turbulence model.

For most transient simulations in this study, between 3 and 10 inner iterations per time step were sufficient to achieve solution convergence. The adopted computational time step is $\Delta t = 0.0001[s]$, which ensures a sufficiently small *CFL* (Courant–Friedrichs–Lewy, $CFL = \langle u \rangle \Delta t / \Delta x$, where Δx is the spatial discretization size) value (less than 2) for most of the computational domain. Additionally, a simulation was performed with a time step of $\Delta t = 0.00005[s]$, resulting in a *CFL* number less than one throughout the domain. The differences between these two cases are very small, as shown in the mesh convergence and time step section. The iteration process is carried out until a steady periodic flow pattern is achieved, and then the simulation is continued to obtain time-averaged data of the flow field.

A schematic diagram of the computational domain and the boundary conditions used in this work are summarized in Figure 1.

Figure 1: Simulation model.

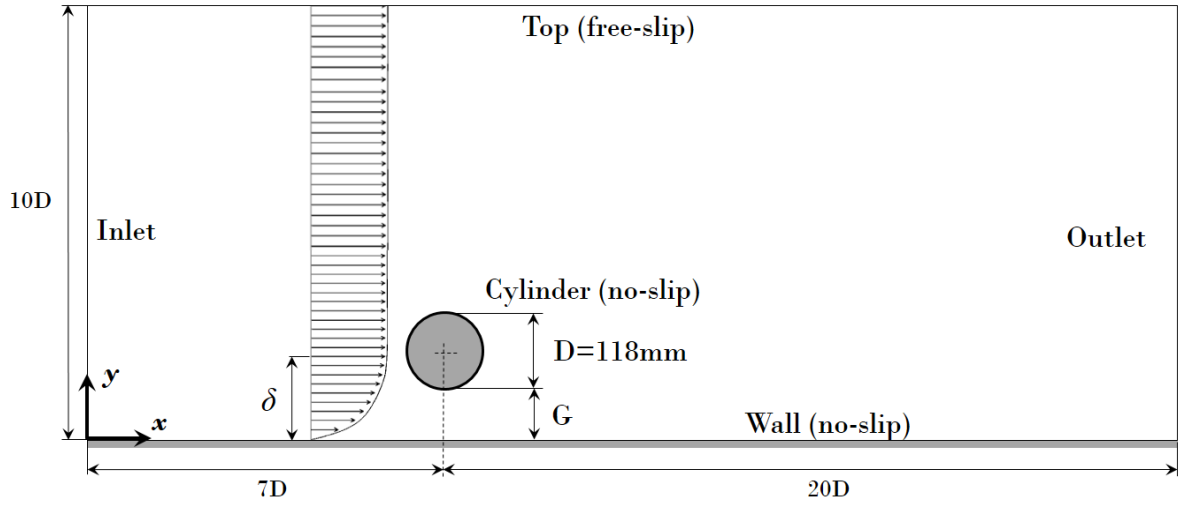

Source: generated by the authors.

3.1 BOUNDARY LAYER MODELING

The experimental tests conducted by Buresti y Lanciotti (1992) were performed with three different types of wind tunnel floor boundary layers, with a relative thickness δ/D ranging from 0.1 to 1.1, at Reynolds numbers ranging from 8.6×10^4 to 2.77×10^5. In this work, the numerical simulations are carried

out using only two boundary layers (BL1 and BL2), as summarized in Table 1.

Table 1: Characteristics of the boundary layers.

	Thickness δ (mm)	Relative thickness δ/D
Boundary layer 1 (BL1)	13	≈ 0.1
Boundary layer 2 (BL2)	130	≈ 1.1

Source: generated by the authors.

To reproduce the boundary layers obtained in the wind tunnel tests by Buresti y Lanciotti (1992) at the cylinder position, numerical simulations were performed with the cylinder removed from the control volume, as this is how they were experimentally obtained. Boundary layer 1 (BL1) is obtained at a distance of seven diameters (7D) from the model's inlet boundary condition when a uniform velocity is imposed (see Figure 2). Therefore, in order to carry out the numerical simulations of Boundary Layer 1, the cylinder will be positioned at a distance of 7D from the inlet of the control volume for each analyzed Reynolds number. For Boundary Layer 2 (BL2), a velocity distribution that satisfies the potential flow law is applied, given by:

$$\langle u \rangle = U_\infty \left(\frac{y}{\delta} \right)^\alpha \qquad (7)$$

Where,

$\langle u \rangle$ is the component of the velocity in the *x* direction at height *y*, U_∞ is the velocity at $y \geq \delta$, *y* is the height relative to the wall, and α is the exponent of the potential flow law. For representing the boundary layer 2, the exponent value is $\alpha = 0.11$. By imposing the velocity profile defined by Eq. (11) as the inlet condition using user-defined functions (UDF) provided by the Ansys Fluent code, the experimental profile (BL2) is obtained again at a position of seven cylinder diameters (7D) from the inlet. The comparison of the profiles for different Reynolds numbers can be seen in Figure 3.

Figure 2: Average velocity profile for the BL1 at x=7D: a) Re=8.6x10^4, b) Re=1.89x10^5 y c) Re=2.77x10^5.

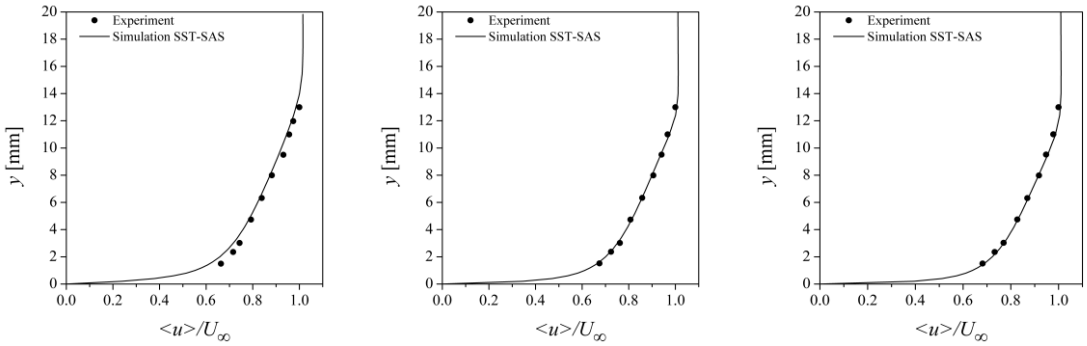

a) b) c)

Source: results of our calculations using the software Fluent Ansys and data obtained from the paper Buresti and Lanciotti (1992).

Figure 3: Average velocity profile for BL2 at x=7D: a) Re=8.6x10^4, b) Re=1.89x10^5 y c) Re=2.77x10^5.

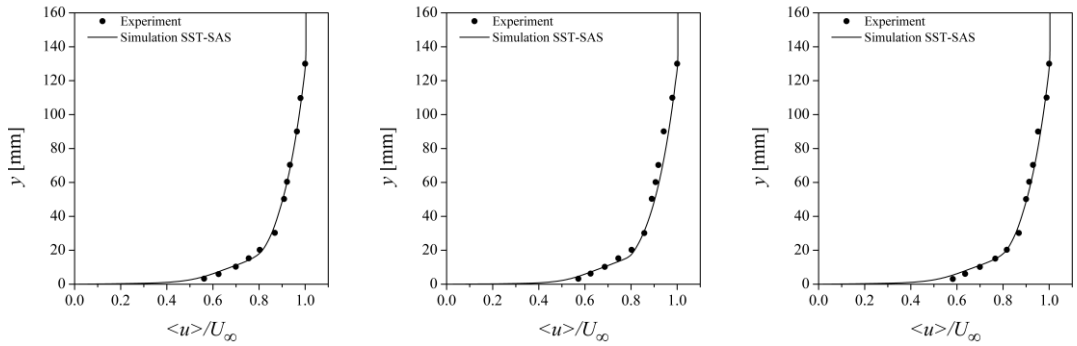

a) b) c)

Source: results of our calculations using the software Fluent Ansys and data obtained from the paper by Buresti and Lanciotti (1992).

3.2 COMPUTATIONAL MESH

The 2D structured multiblock meshes were generated using the Ansys ICEM CFD software. The mesh resolution around the cylinder is similar to the mesh used for an isolated circular cylinder in free flow by Menter et al. (2003), which demonstrated the capability of the SST-SAS model to capture turbulent structures. An example of the 2D mesh is shown in Figure 4, with a refinement near the cylinder and the ground (to capture the boundary layers), ensuring a spatial resolution of $y^+ < 1$ with 20 and 30 elements to reproduce the boundary layer. For the discretization of the cylinder, 160 equidistant elements were used, resulting in a total mesh with 27219 hexahedral elements.

Figure 4: Mesh near the cylinder and the wall.

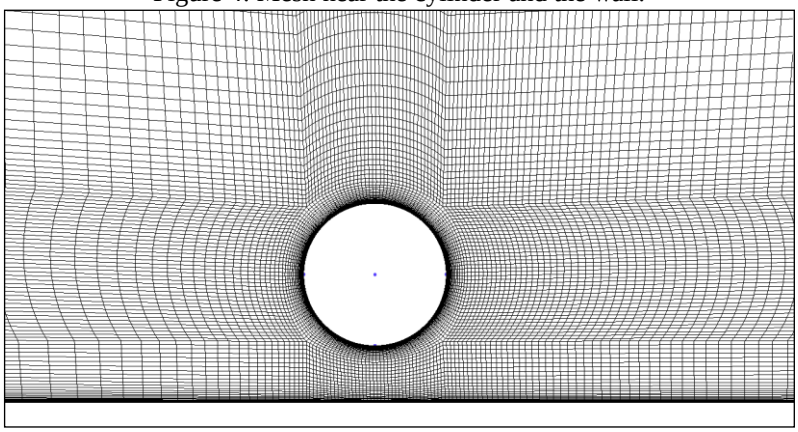

Source: obtained from our own model.

In order to investigate the effect of the proximity of a cylinder to a plane wall, five different meshes were created, one for each G/D ratio of 0.2, 0.3, 0.4, 0.8, and 1.5. The number of elements in the *y* direction remains the same (121 elements), but the number of elements between the cylinder and the wall changes as the cylinder moves closer or farther away from the ground (the opposite occurs with the elements between the cylinder and the upper part), ensuring a similar aspect ratio of the elements for each G/D ratio.

In addition to these five meshes for the main part of the study, two additional meshes with different spatial resolutions were created to examine the dependence of the simulations on the meshes.

3.3 MESH AND TIME STEP CONVERGETION

A mesh and time step convergence analysis was performed at Re = 8.6×10^4 and a cylinder-to-wall position of G/D=1.5, as shown in Table 2. The mean drag and lift coefficients, as well as the Strouhal number values, were compared. The case defined as *M2* in Table 2 indicates the spatial and temporal resolution adopted as the reference in the present work. A comparison of the influence of spatial resolution in the *x* and *y* directions is shown for cases *M1*, *M2*, and *M3*. To achieve a constant mesh refinement ratio, in the *M1* case, the number of cells in each direction (*x* and *y*) was set such that the reference case *M2* resulted in 50% more cells in each direction than in the *M1* mesh. The same for the *M3* case, the number of cells in each direction was increased by 50% compared to the reference mesh (*M2*). It can be observed that convergence is achieved for Cl and St, but it is not as clear for the Cd values. However, the difference between the *M2* and *M3* cases is smaller than between the *M1* and *M2* cases, suggesting some degree of mesh convergence for Cd.

The time step used for mesh convergence was set to $\Delta t = 0.0001[s]$, which is the same time step used by Menter et al. (2003). To ensure time step convergence, the reference case *T1* is compared to *T2*. In the *T2* case, a time step of $\Delta t = 0.00005[s]$ was used, which assure a *CFL* number less than 1 throughout

the simulation domain. The differences between the *T1* and *T2* cases demonstrate adequate time step convergence, as shown in Table 2.

Table 2: Summary of simulations with different spatial and temporal resolution (Re=8.6x10^4, G/D=1.5).

Case	Cells	*Δt*	*CD*	*CL*	*St*
Spatial resolution (Δx, Δy)					
M1	11934	0.0001	1.155	0.089	0.269
M2	27219	0.0001	1.189	0.071	0.280
M3	62353	0.0001	1.164	0.040	0.280
Temporal resolution (Δt)					
T1	27219	0.0001	1.189	0.071	0.280
T2	27219	0.00005	1.182	0.085	0.279

Source: generated with the results of our own calculations.

3.4 BOUNDARY CONDITIONS

At the inlet of the domain, a constant flow (uniform for boundary layer 1 and a velocity profile for boundary layer 2) with a low turbulence level (corresponding to a turbulence intensity of 0.9% and a turbulent viscosity ratio equal to unity) is applied for each simulated flow (Re = 8.6x10^4, 1.89x10^5, and 2.77x10^5). At the outlet of the simulation domain, a zero flow diffusion condition is applied for all variables. This condition is defined as an "outflow" boundary condition in Fluent. For the upper boundary of the domain, a free-slip wall condition is specified. Regarding the cylinder and wall conditions, a no-slip condition is considered, meaning a zero velocity.

4 RESULTS

The flow around a cylinder is simulated considering the proximity of a plane wall. The study is conducted for various separation ratios (G/D=0.2, 0.3, 0.4, 0.8, and 1.5), two different boundary layers (BL1 and BL2), and different Reynolds numbers (Re=8.6x10^4, 1.89x10^5, and 2.77x10^5). A summary of the analyzed cases is shown in Table 3.

Table 3: Cases simulated.

Case	G/D	δ/D	Re
2D-SST-SAS	0.2, 0.3, 0.4, 0.8 ,1.5	0.1 , 1.1	8.6x10^4, 1.89x10^5, 2.77x10^5

Source: generated by the authors.

This investigating focused on the forces on the cylinder (drag and lift), the frequencies and characteristics of vortex shedding for different separations of the cylinder with the plane wall. The results obtained from these simulations are compared with experimental data provided by Buresti y Lanciotti (1992).

4.1 MEAN DRAG AND LIFT COEFFICIENTS

The mean flow characteristics were calculated over a 1 s-long period of time. This time duration is equivalent between 20 and 30 vortex shedding at $Re=8.6x10^4$. Figure 5 and

Figure 6 compare the mean drag and lift coefficients as a function of the cylinder-to-wall separation, evaluated numerically, with experimental results obtained at the same Reynolds number by Buresti y Lanciotti (1992). The drag (*CD*) and lift (*CL*) coefficients are defined as: $CD=FD/(0.5\rho U\infty 2A)$ where *FD* is the drag force exerted on the cylinder, and A is the projected area of the cylinder; $CL=FL/(0.5\rho U\infty 2A)$, where *FL* is the lift force exerted on the cylinder.

Figure 5: Mean drag coefficient as a function of G/D.

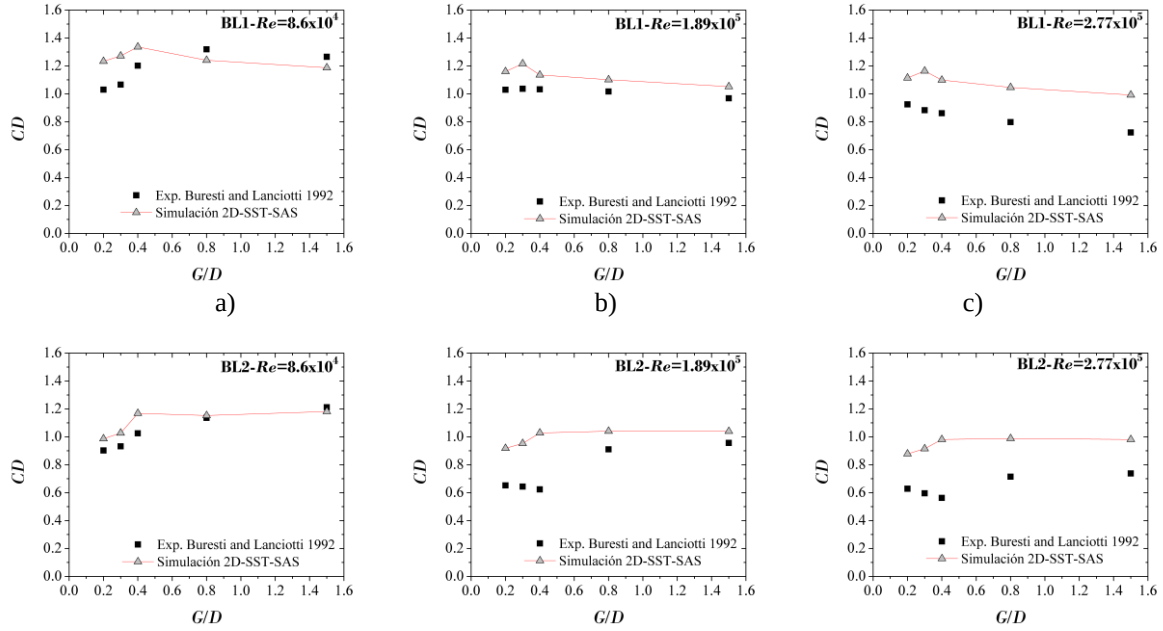

Source: results of our calculations using the software Fluent Ansys and data obtained from the paper by Buresti and Lanciotti (1992).

Figure 6: Mean lift coefficient as a function of G/D.

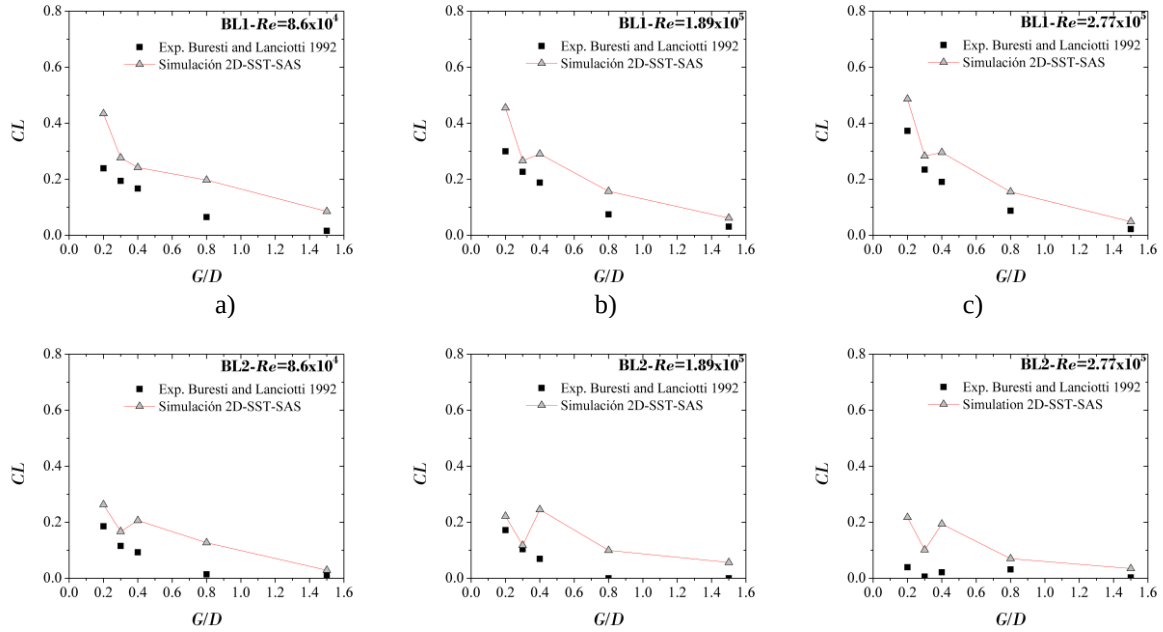

Source: results of our calculations using the software Fluent Ansys and data obtained from the paper by Buresti and Lanciotti (1992).

In a general way, it can be observed from Figure 5 and

Figure 6 that the results obtained through numerical simulation are reasonably close to the experimental data. The numerical simulations demonstrate that both the drag coefficient (*CD*) and the lift coefficient (*CL*) depend on the separation ratio (G/D) and are affected by the wall boundary layer. Another aspect that can be established is that the 2D-SST-SAS model generally exhibits an over-prediction of the results for both *CD* and *CL*, with the largest differences observed in the Cd values. Additionally, it can be observed from Figure 5 and

Figure 6 that the results for when the cylinder is far from the plane wall (a condition where the effects of the wall become negligible, $CL \approx 0$), the 2D-SST-SAS model provides a better approximation to the data obtained by Buresti and Lanciotti. One possible explanation for the lack of accuracy in evaluating the trends when the cylinder is close to the wall (G/D=0.2-0.4) could be that the 2D-SST-SAS simulations fail to reproduce the cessation of vortex shedding, an effect that occurs when the cylinder is located near those G/D ratios (see following section Strouhal number and vortex shedding).

4.2 STROUHAL NUMBER AND VORTEX SHEDDING

The Strouhal number is defined as $St=fD/U\infty$, where f is the vortex shedding frequency [Hz] obtained from the fluctuating lift force. The predicted St by the 2D-SST-SAS simulations for the Re number of $Re=8.6x10^4$ is shown in Figure 7.

Figure 7: Variation of the Strouhal number (*St*) as a function of the separation with the wall at Re=8.6x10^4.

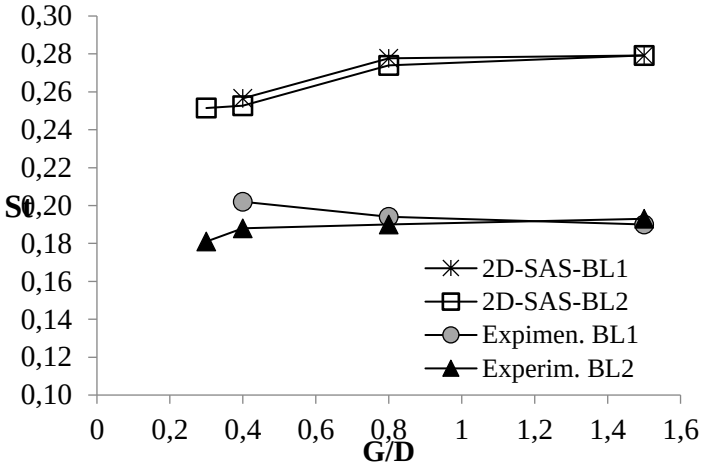

Source: results of our calculations using the software Fluent Ansys and data obtained from the paper by Buresti and Lanciotti (1992).

It can be observed that the Strouhal number values obtained by the 2D-SST-SAS model are slightly higher (overestimated) compared to the data from the experimental tests by Buresti and Lanciotti.

The vortex shedding from the cylinder can be identified through the lift coefficient or by examining velocity contours, as shown in Figure 8.

Figure 8 depicts the temporal variations of the lift coefficients and instantaneous velocity contours (at a given instant) for the case of boundary layer 1 and Re=8.6x10^4 at different distances of the wall. It can be noted that as the cylinder approaches the wall, the suppression (or cessation) of vortex shedding does not occur, even for G/D=0.2, where it is expected that vortex shedding completely ceases according to the experiments. Due to the absence of vortex shedding suppression for G/D=0.2, an additional study was conducted for G/D=0.1, resulting in the suppression of vortex shedding, as observed in Figure 9.

This reduction in the critical separation value for the 2D-SST-SAS case may be attributed to the larger amplitude of lift fluctuations, indicating a stronger vortex shedding force behind the cylinder. As a result, suppressing these vortices becomes more challenging, leading to a lower (G/D)c value. The same behavior is observed for the other Reynolds numbers considered and for the other boundary layer analyzed.

Table 4: Critical value G/D for suppression of vortex shedding.

Re	δ/D	G/D$_c$ (2D-SST-SAS)	G/D$_c$ Buresti and Lanciotti 1992
8.6x10^4	0.1	0.2	0.4
	1.1	0.2	0.3
1.89x10^5	0.1	0.2	-
	1.1	0.2	-
2.77x10^5	0.1	0.2	-
	1.1	0.2	-

Source: results of our calculations using the software Fluent Ansys and data obtained from the paper by Buresti and Lanciotti (1992).

Figure 8: Time variation of the lift coefficient (Cl) and contours of the magnitude of instantaneous velocity (m/s) for BL1 and Re=8.6x10^4: a) G/D=1.5; b) G/D=0.8; c) G/D=0.4; d) G/D=0.3; e) G/D=0.2.

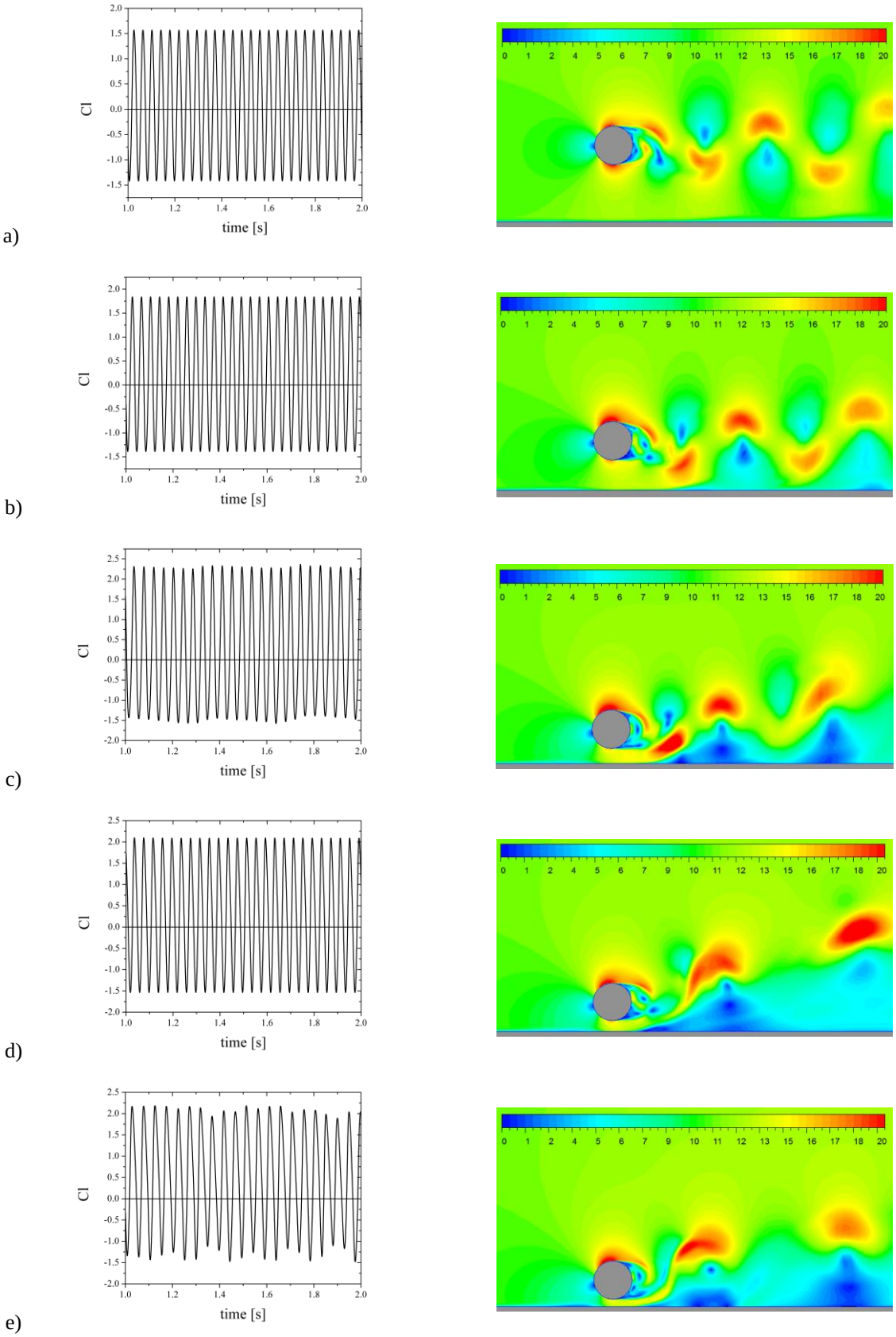

Source: results of our calculations using the Fluent Ansys software.

A summary of the critical value for suppression of vortex shedding (G/Dc) is given in Table 34 for the three Reynolds numbers and for the two boundary layers of the ground considered in the present study. By analyzing the effect of Reynolds number on vortex shedding suppression, it is observed from Table 34 that G/Dc predicted by 2D-SST-SAS remains unchanged with the Re. Also, the numerical study indicates that the critical gap does not show a dependency on the incident boundary layer thickness

Figure 9: Temporal variation of the drag and lift coefficients for BL1, Re=8.6x10^4 and G/D=0.1: Cd (solid line), Cl (dashed line).

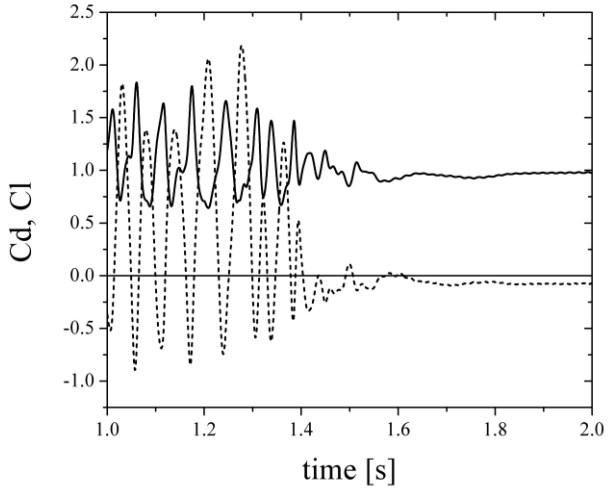

Source: results of our calculations using the Fluent Ansys software.

5 CONCLUSION

Two-dimensional numerical simulations using the SST-SAS turbulence model were performed to investigate the flow around a circular cylinder considering the proximity to a plane wall. The simulations were conducted for five different cylinder-to-wall distances (G/D=0.2, 0.3, 0.4, 0.8, and 1.5), two wall boundary layers (BL1 and BL2), and three different Reynolds numbers (Re=8.6x10^4, 1.89x10^5, and 2.77x10^5). The comparison of these results with wind tunnel experiments available in the literature led to several relevant conclusions.

The simulations demonstrated that the drag coefficient (*CD*) and lift coefficient (*CL*) is dependent on the separation ratio (G/D) with the wall and the boundary layer thickness. Additionally, the results indicated that the 2D-SST-SAS model provided a better approximation to the experimental data when the cylinder was far from the wall. Another important conclusion was that the Strouhal number values obtained from the numerical simulations were slightly higher than the experimental values for different cylinder separation of the plane wall. On the other hand, the 2D-SST-SAS simulations failed to reproduce the cessation of vortex shedding, an effect that occurs when the cylinder is located near the wall.

Based on these conclusions, it can be inferred that the SST-SAS used for two-dimensional models may be more reliably applied on isolated cylinders rather than considering the proximity to a plane wall.

REFERENCES

Bearman, P.W., Zdravkovich, M.M., Flow around a circular cylinder near a plane boundary. *Journal of Fluid Mechanics*, 89, 33-47, 1978.

Buresti, G., Lanciotti, A., Mean and fluctuating forces on a circular cylinder in cross flow near a plane surface. *Journal of Wind Engineering and Industrial Aerodynamics*, 41, 639-650, 1992.

Egorov, Y., Menter, F., Development and application of SST-SAS turbulence model in the *DESIDER project. Notes on Numerical Fluid Mechanics and Multidisciplinary Design* 97, 261- 270, 2008.

Grioni, M., Elaskar, S., Mirasso, A., Simulación de flujo transitorio 2D alrededor de un cilindro circular horizintal considerando el efecto suelo, *Mecánica Computacional*, 35, pp. 873-885, 2017.

Grioni, M., Elaskar, S., Mirasso, A., Análisis transitorio de la interferencia de flujo entre dos cilindros circulares en disposición tándem, *Mecánica Computacional*, 36, pp. 1195-1204, 2018a.

Grioni, M., Elaskar, S., Mirasso, A., Scale-Adaptive Simulation of Flow around a Circular Cylinder near a Plane Boundary, *Journal of Applied Fluid Mechanics*, 6, pp. 1477-1488, 2018b.

Grioni, M., Elaskar, S., Mirasso, A., Bruel, P. Interferencia de flujo entre cilindros circulares en disposición tándem cercanos al suelo, *Mecánica Computacional*, 37, pp. 1065-1074, 2019.

Grioni, M., Elaskar, S., Mirasso, A., A numerical study of the flow interference between two circular cylinders in tandem by scale-adaptive simulation model, *Journal of Applied Fluid Mechanics*, 13, pp. 169–183, 2020.

Grioni, M., Bruel, P., Elaskar, S. and Mirasso, A., An application of the scale adapted simulation to the unsteady flow across a tube bundle. *International Journal of Heat and Fluid Flow*, 96, 109007, 2022a.

Grioni, M. Elaskar, S., Bruel, P., Mirasso, A., Comparación de algoritmos de acoplamiento velocidad-presión para problemas no estacionarios del flujo alrededor de un cilindro circular, 2022 *IEEE biennial congress of argentina* (ARGENCON), pp. 1-8, 2022b.

Lei, C., Cheng, L., Kavanagh, K., Re-examination of the effect of a plane boundary on force and vortex shedding of a circular cylinder. *Journal of Wind Engineering Industrial Aerodynamics*, 80, 263–286, 1999.

Menter, F.R., Two-equation eddy viscosity models for engineering applications. *AIAA Journal*, 32(8): 269–289, 1994.

Menter, F.R., Kuntz, M., Bender, R., A scale-adaptive simulation model for turbulent flow predictions. *AIAA Paper 2003-0767*, Reno, Nevada, USA, 2003.

Menter, F.R. and Egorov, Y., A scale-adaptive simulation model using two-equation models, *Paper AIAA 2005-1095*, Reno, Nevada, USA, 2005.

Menter, F., Egorov, Y., The scale-adaptive simulation method for unsteady turbulent flow predictions. part 1: theory and model description. *Flow, Turbulence and Combustion*. 85 (1), 113–138, 2010.

Patankar, S.V., Numerical heat transfer and fluid flow. Hemisphere, Washington, DC, USA, 1980.

Spalart, P.R., Strategies for turbulence modelling and simulations. *International Journal of Heat and Fluid Flow*, 21, 252-263, 2000.

Strelets, M., Detached eddy simulation of massively seperated flows. *AIAA* Pap. 2001-0879, 2001.

Taniguchi, S., Miyakoshi, K., Fluctuating fluid forces acting on a circular cylinder and interference with a plane wall. *Experiments in Fluids*, 9, 197-204, 1990.